*Catalysis Letters, Vol. 115, Nos. 1–2, May 2007 (© 2007)*
DOI: 10.1007/s10562-007-9078-9


# Sulfated zirconia in SBA-15 structures with strong Brønsted acidity as observed by $^1$H MAS NMR spectroscopy

Volkan Degirmenci,[a] Özlen Ferruh Erdem,[b] Aysen Yilmaz,[c] Dieter Michel,[b] and Deniz Uner[a,*]

[a]*Department of Chemical Engineering, Middle East Technical University, Ankara 06531, Turkey*
[b]*Institute of Experimental Physics II, University of Leipzig, D-04103 Leipzig, Germany*
[c]*Department of Chemistry, Middle East Technical University, Ankara 06531, Turkey*

Received 26 February 2007; accepted 28 February 2007

In order to prepare high surface area highly acidic catalysts, different weight loadings of $ZrO_2$ were incorporated in the SBA-15 structures which are subsequently sulfated by treating in 0.25 M $H_2SO_4$. The catalysts were characterized by means of TEM, XRD, $N_2$ adsorption, and $^1$H MAS NMR. Brønsted type acidities of sulfated zirconia included SBA-15 materials were identified by a sharp $^1$H MAS NMR line at 10.6 ppm. The highest acidity was obtained in the 25 mol% $ZrO_2$ included SBA-15 catalyst with a BET surface area of 246 $m^2$/g.

**KEY WORDS:** sulfated zirconia; super acid catalysts; $^1$H MAS NMR; SBA-15; mesoporous silica.

## 1. Introduction

Sulfated zirconia (S-$ZrO_2$) has been extensively studied due to its strong acidity for the activation of C–C and C–H bonds of alkanes [1,2] and especially for the isomerization of small hydrocarbons [3]. However, there is a debate on the interpretation of the origin of the superacidic property ascribed to sulfated zirconia. Some authors suggest that the catalyst does not possess superacid strength [4,5] but catalytically active due to the reaction path via a less energy intensive bi-molecular mechanism in *n*-butane isomerization [6–8]. On the other hand, there are reports on the superacid properties of sulfated zirconia debating on the origin of high catalytic activity either by the combination of Brønsted and Lewis sites or only Brønsted acid sites [9].

The conventional sulfated zirconia lacks pore volume with typical surface areas of ca. 100 $m^2$/g. Since the catalytic activity strongly depends on surface area, much effort has been spent in order to prepare a high surface area sulfated zirconia. In this sense mesoporous silicas have attracted increasing interest due to its extensively high surface area (ca. 1000 $m^2$/g), large pore volume, and a uniform hexagonal array of pores [10–13]. The silanol groups on the surface of these materials are non-acidic or slightly acidic. The potential combinations of the mesoporous silicas and the superacidic sulfated zirconia should greatly enhance the catalytic capabilities of both materials for the applications where strong acidity is essential.

*To whom correspondence should be addressed.
E-mail: uner@metu.edu.tr

Different techniques have been reported to achieve a combination of sulfated zirconia and MCM-41 type mesoporous silicas [14,15]. MCM-41 is prepared in a basic medium and it is difficult to maintain the crystal structure in strong acidic media. Moreover, they have the problem of losing their uniform pore structure after calcination [16], or showing a lack of catalytic activity [17,18]. SBA-15 type mesoporous materials have higher stability than other mesoporous silicas due to their thicker walls, which enables the introduction of other metals into the framework. Therefore, it is a suitable material to host zirconium. It has been reported that sulfated zirconia may be impregnated into SBA-15 by means of the incipient wetness method [19,20]. The impregnation of zirconia into the SBA-15 support is a straightforward technique, but it is difficult to obtain uniformly distributed zirconia on the support. The introduction of the zirconia precursor simultaneously with the silicon precursor in the preparation of SBA-15 is a better way to obtain a fine distribution of zirconia [21,22].

In this study the effect of the inclusion of sulfated zirconia to SBA-15 on the acidic properties is investigated by means of $^1$H MAS NMR spectroscopy, because the proton chemical shift is sensitive to the electronic environment [23,24] and the $^1$H chemical shifts are known to be correlated with the acidic strength of the surface OH groups [25–27]. $^1$H MAS NMR investigations on conventional zirconia and sulfated zirconia samples have been reported by Riemer *et al.* [28]. It is reported that sulfate-free $ZrO_2$ shows a $^1$H NMR line at 3.86 ppm and a weaker signal at 1.60 ppm. On the other hand, the sulfated sample is found to be

dominated by a single line at 5.85 ppm. Thus, the sulfate modification induces a very significant downfield shift of ca. 2 ppm that suggests a strongly enhanced proton acid strength relative to pure $ZrO_2$, i.e. the OH groups developed a high protonic acidity owing to the high electronegativity of $Zr^{4+}$.

## 2. Experimental

### 2.1. Synthesis of catalysts

Pure, $ZrO_2$ included, and $SO_4^{2-}/ZrO_2$ modified SBA-15 type catalysts were prepared according to literature [29,30]. In order to prepare pure SBA-15 molecular sieve, 9 ml of tetraethyl orthosilicate (TEOS) was added to 150 ml of 1.5 M HCl solution containing 4 g of triblock poly(ethylene oxide)–poly(propylene oxide)–poly(ethylene oxide) ($EO_{20}$–$PO_{70}EO_{20}$, Aldrich). The mixture was stirred for 24 h at 313 K and was allowed to react at 373 K overnight in Teflon bottles. The solid material obtained after filtering was finally calcined in airflow at 773 K for 5 h. In the preparation of the $ZrO_2$ included SBA-15, zirconia was introduced in solution simultaneously with TEOS in the form of $ZrOCl_2 \cdot 8H_2O$ at four different loadings: 5, 15, 25, and 30 mol% $ZrO_2$ with respect to the content of $SiO_2$. Finally, the sulfated catalysts were prepared by sulfating in a 0.25 M $H_2SO_4$ solution.

### 2.2. Characterization of catalysts

The X-ray diffractograms were recorded by means of a Rigaku X-ray diffractometer (30 kV, 15 mA) with a miniflex counter using a Cu K$\alpha$ radiation ($\lambda = 1.54$Å). Diffraction patterns were collected at ambient temperature in the $2\theta$ range of 1–3° at a scanning rate of 0.2° $min^{-1}$ in steps of 0.005° and in the $2\theta$ range of 10–70° at a scanning rate of 1 $min^{-1}$ in steps of 0.05°. TEM images were taken on a FEI T20 electron microscope operating at 200 V. The specimens were dispersed in ethanol and placed on holey copper grids. The surface areas were measured using nitrogen adsorption isotherms at −196 °C on a Micromeritics ASAP 2000 gas sorption and porosimetry system. The samples were prepared for measurement by degassing at 150 °C for 24 h. Surface areas were calculated by the BET (Brunauer–Emmett–Teller) method and the pore size distributions were determined by using the BJH (Barrett–Joyner–Halenda) method.

$^1$H MAS NMR experiments were performed at a 400 MHz Bruker AVANCE spectrometer using a MAS probe with an outer rotor diameter of 7 mm. The measurements were performed using the solid echo pulse sequence; the proton 90° pulse length was 3.4 $\mu$s. $^1$H MAS NMR spectra of the samples were collected for the hydrated and dehydrated materials. The $^1$H MAS NMR experiments of the catalysts in the hydrated state were performed by directly filling the catalysts into the 7 mm MAS rotor without any prior treatment. In order to dehydrate the samples, they were placed in special NMR tubes suitable for MAS, connected to a vacuum line, and then heated up to 473 K in steps of 10 K. After a vacuum of $10^{-3}$ bar is achieved, the system was heated up to 573 K where it was kept there for 24 h. After this pretreatment *in vacuo*, the cylindrical glass tubes were sealed off under vacuum conditions. The sealing symmetry was carefully controlled in a way that a fast sample rotation was possible. Then the sealed glass tubes containing the dehydrated samples were placed into the 7 mm MAS rotor. Details of this special preparation of NMR samples suitable for MAS are described, for instance, in Ref. [31,32].

## 3. Results and discussion

### 3.1. X-ray diffraction

X-ray diffraction patterns of pure and zirconia included SBA-15 samples are shown in figure 1. Pure and 5–15 mol% $ZrO_2$ included SBA-15 samples exhibit two lines at ca. $2\theta$ = 1.6° and 1.8° corresponding to diffraction lines from (110) and (200) planes of SBA-15. The disappearance of the lines in the small-angle region at higher zirconia loadings (20–30 mol% $ZrO_2$/SBA-15) indicates the loss of uniform mesostructure with respect to the increase in the zirconia content.

In the wide angle region the catalysts below 25 mol% $ZrO_2$ loading exhibit no diffraction lines, indicating that zirconia is distributed uniformly within the structure. In the wide angle XRD pattern of the catalyst with 25 mol% $ZrO_2$ content, a diffraction line at $2\theta$ = 30° were observed, which corresponds to the tetragonal crystalline zirconia. In 30 mol% $ZrO_2$ loading, two additional lines at ca. 50° and 58° were also appeared, corresponding to the tetragonal and monoclinic zirconia crystals. The XRD lines of crystalline zirconia appeared in the samples with high zirconia contents, ca. ≥25 mol%. Thus, for catalysts at ca. ≥25 mol% $ZrO_2$ contents, zirconia is not distributed finely within the structure, but the zirconia crystals were formed. At these loadings, small angle XRD lines at $2\theta$ = 1.6° and 1.8° also disappeared, indicating that the long range order of the structure was lost upon the agglomeration of zirconia precursor to form crystalline phases.

### 3.2. Transmission electron microscopy

Figure 2 shows the TEM images of the non-sulfated (figure 2a–c) and sulfated catalysts (figure 2d–f) with 0–25 mol% $ZrO_2$ loading. Pure SBA-15 exhibits hexagonally ordered arrays of uniform mesopores (figure 2a). The uniform mesostructure was not influenced during the sulfation process for pure SBA-15 (figure 2d). As observed in figure 2b, when the zirconia loading was

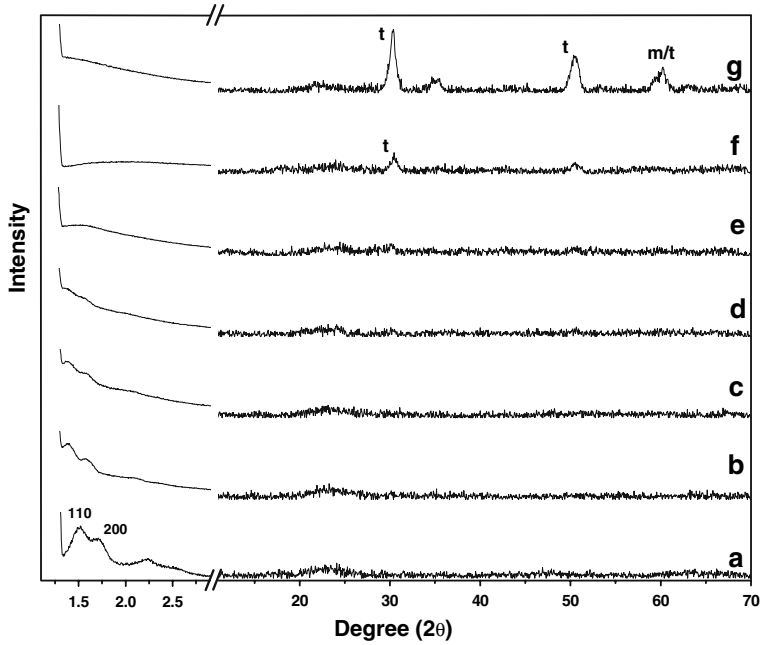


Figure 1. Small angle and wide angle XRD patterns of non-sulfated SBA-15 with (a) 0 (b) 5 (c) 10 (d) 15 (e) 20 (f) 25 (g) 30 mol% $ZrO_2$ loading.

increased to 15 mol%, mesostructure was still retained. Zirconia could not be distinguished in the TEM images, indicating a high dispersion of zirconia in the mesostructure, in agreement with the wide angle XRD patterns at these loadings. After sulfation treatment of the 15 mol% $ZrO_2$ included catalyst, the structure exhibited uniformity to some extent (figure 2e). At 25 mol% zirconia loading, however, a drastic change was observed (figure 2c and f). The ordered arrays of mesopores were not seen in the non-sulfated and the sulfated sample. Although the XRD patterns indicated the formation of the zirconia crystals at 25 mol% loading, no crystals could be distinguished in the TEM image.

### 3.3. $N_2$ adsorption

The structural parameters of the catalysts obtained from BET analysis were presented in table 1. SBA-15

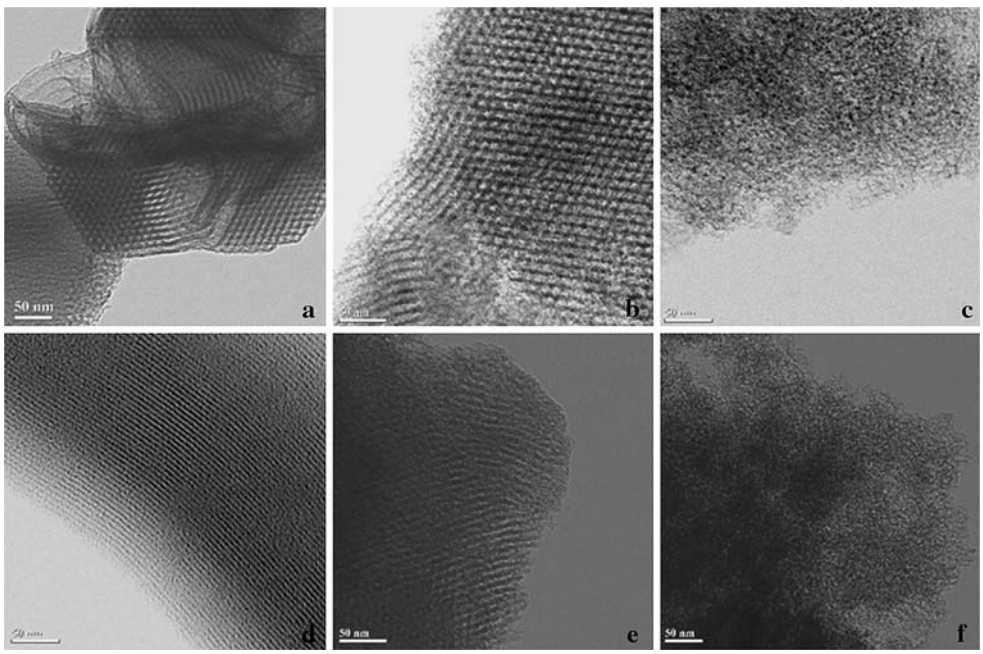


Figure 2. TEM images of non-sulfated SBA-15 with (a) 0 (b) 15 (c) 25 mol% $ZrO_2$ loading and sulfated SBA-15 with (d) 0 (e) 15 (f) 25 mol% $ZrO_2$ loading.

Table 1
BET surface area, BET single point total volume of pores and average pore diameters of the non sulfated and sulfated $ZrO_2$/SBA-15

| Catalysts | BET surface area ($m^2$/g) | Pore diameter (Å) | Pore volume (cc/g) |
|---|---|---|---|
| SBA-15 | 773 | 71.2 | 1.18 |
| 5 mol% $ZrO_2$-SBA-15 | 733 | 77.5 | 1.34 |
| 20 mol% $ZrO_2$-SBA-15 | 574 | 103.5 | 1.55 |
| 5 mol% Sulfated $ZrO_2$-SBA-15 | 313 | 54.5 | 0.43 |
| 15 mol% Sulfated $ZrO_2$-SBA-15 | 284 | 55.9 | 0.40 |
| 25 mol% Sulfated $ZrO_2$-SBA-15 | 246 | 55.5 | 0.34 |

exhibits a BET surface area of 773 $m^2$/g, confirming the highly ordered mesostructure in good agreement with the TEM results. Zirconia included catalysts have lower surface areas than pure SBA-15 ranging between 733 $m^2$/g and 574 $m^2$/g. Sulfated catalysts show BET areas in between 313–246 $m^2$/g.

Figure 3(a) shows the pore size distributions of catalysts before sulfation. The narrow pore size distribution of SBA-15 around 10 nm indicates its highly ordered mesostructure. As the zirconia content increases, the pore size distribution was broadened. This is in agreement with the XRD patterns and the TEM images that the increase in zirconia content reduces the uniformity of the structure. The pore size distribution of the sulfated samples is wider, in 2–8 nm pore size range (figure 3b).

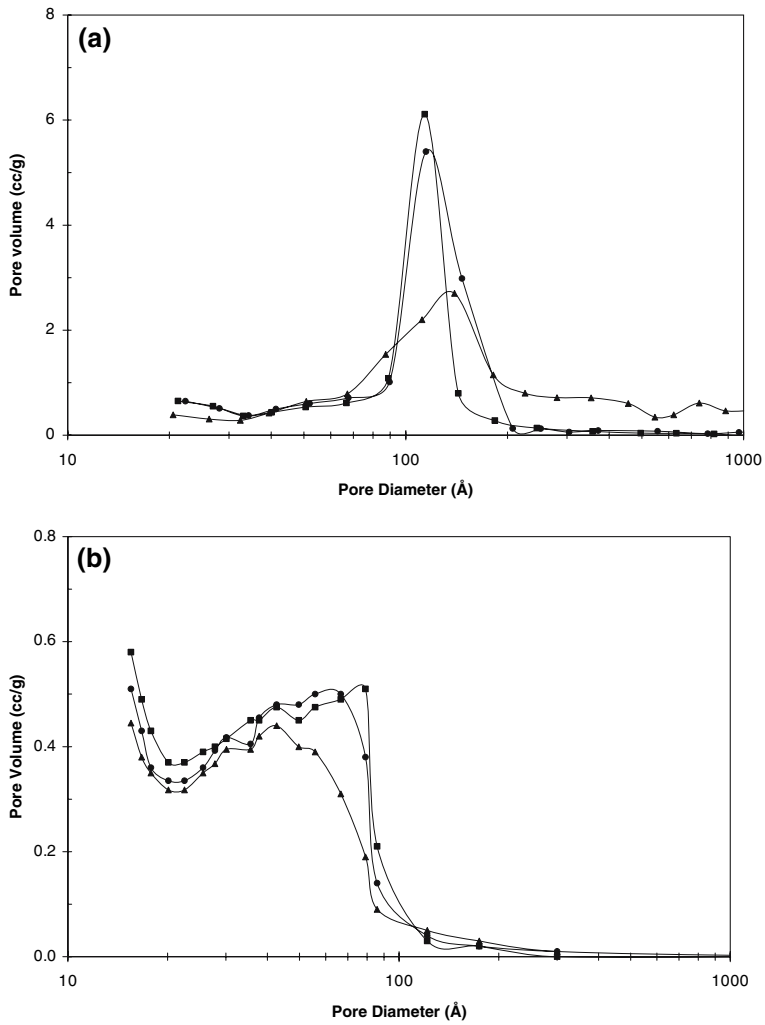


Figure 3. (a) BJH pore size distribution of non-sulfated SBA-15 with 0 (■), 5 (●) and 20 (▲) mol% $ZrO_2$ loading. (b) BJH pore size distribution of sulfated SBA-15 with 5 (■), 15 (●) and 25 (▲) mol% $ZrO_2$ loading.

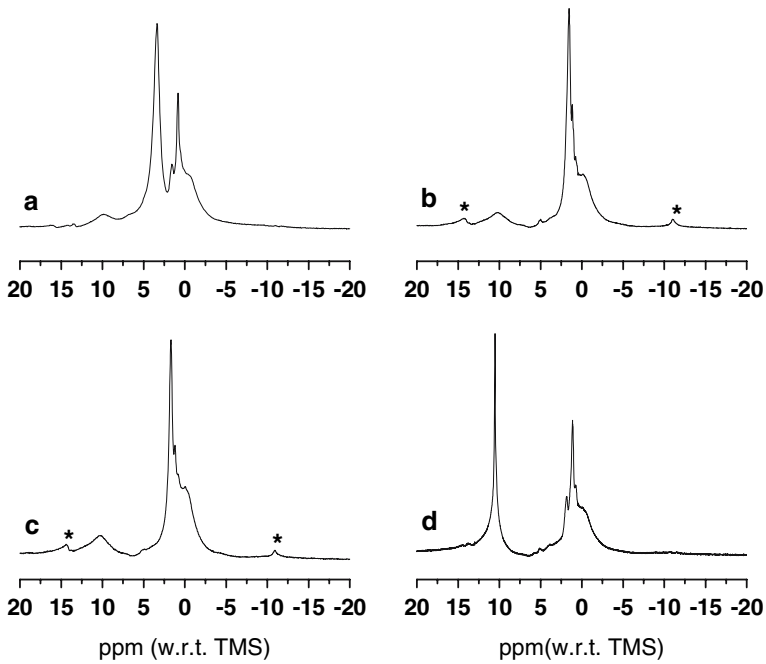


Figure 4. $^{1}$H MAS NMR taken at AVANCE-400 with an MAS frequency of 5 kHz at 300 K for (a) pure hydrated SBA-15, (b) pure dehydrated SBA-15, (c) dehydrated SBA-15 with 5% $ZrO_2$, (d) dehydrated sulfated SBA-15 with 5% $ZrO_2$. *Stands for the spinning side bands.

### 3.4. *$^{1}$H MAS NMR spectroscopy*

In the present $^{1}$H MAS NMR measurements, we compared the spectra of hydrated and dehydrated SBA-15 materials with modified SBA-15 mesoporous catalysts. The modifications include co-precipitation with zirconia and then the sulfation of the zirconia samples with $H_2SO_4$ as described above. In figure 4(a) and (b) the proton NMR spectra are shown for hydrated and dehydrated SBA-15 materials without any further modification. The dehydrated samples reveal an overlap of various resonance lines. In the shift range of structural OH groups, the deconvoluted $^{1}$H MAS NMR spectra reveal four distinct resonance lines at −0.5, 0.7 (very weak shoulder), 1.2, and 1.8 ppm relative to liquid TMS. Prior to dehydration, an additional line at ca. 3.5 ppm, attributed to bound water [33], was also observed. It is known from the previous work [23,34,35] on MCM-41 that the asymmetric shape of these signals is a hint for the presence of different types of silanol groups, such as isolated and geminal SiOH groups and internal SiOH groups.

The chemical shift range between 1.2 ppm and 2.2 ppm is typical for silanol groups in most of the zeolites (Hunger *et al.* [34] and references therein). According to Trèbosc *et al.* [23], the isolated, i.e. non-hydrogen bonded, single and/or geminal SiOH groups are not detectable directly at their usual position around 1.8 ppm due to the fast proton exchange. In our SBA-15 material, the intensity of 1.2 ppm line does not change appreciably, but the intensity of the line at 1.8 ppm is increased upon removal of water (figure 4a and b). We interpret this situation as the decrease of intensity at 1.8 ppm line under hydrated conditions due to the fast exchange with bound water. On the other hand, species giving rise to 1.2 ppm line is not interacting with adsorbed water. The intensities and the shift of the weak line at 0.7 ppm and the peak at −0.5 ppm were also not changed in the dehydrated samples. We interpret this as the inaccessibility of these proton sites to water. Furthermore, a relatively weak broad line at ca. 10 ppm is observed which is not altered in the modification process. This line was also not accessible to the proton exchange with OH groups and water. We interpret this strong shift in terms of a strong non-symmetric hydrogen bond [36,37] to inaccessible SiOH groups in the walls of the SBA-15. The origin of the −0.5 and 0.7 ppm lines in pure SBA-15 is not completely clear so far, but this uncertainty does not influence our further interpretation as to be still discussed.

We have clearly observed that for our $ZrO_2$/SBA-15 samples without sulfation the $^{1}$H MAS NMR spectra for the dehydrated samples are practically the same as for the non-modified SBA-15 samples (figure 4b and c). However, clear changes are measured for sulfated $ZrO_2$/SBA-15 samples (figure 4d). An intense line appears at 10.6 ppm that was not detected in all other samples without sulfation. This line can be related to superacid sites, which are introduced by the sulfation treatment. The intensity of this line increases with the $ZrO_2$ content ca. up to 25% (table 2). A further increase in the $ZrO_2$ content causes a decrease in the relative intensity of this line. This is better observed if we compare the spectra for the dehydrated sulfated samples with those for the

Table 2
Relative intensities of the line at 10.6 ppm from the deconvoluted $^1$H MAS NMR spectra for different zirconia contents[a]

| $ZrO_2$ mol% of the sulfated sample | 0 | 5 | 15 | 25 | 30 |
|---|---|---|---|---|---|
| Relative intensity (%) | 0 | 6 | 7 | 23 | 15 |

[a] The relative intensities were estimated from the area under these lines with respect to the total spectrum.

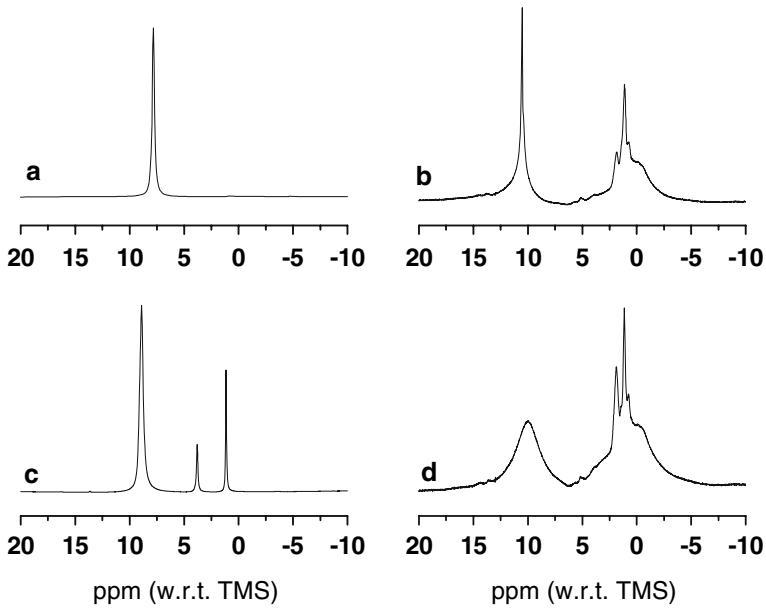


Figure 5. $^1$H MAS NMR taken at Avance-400 with MAS spinning frequency of 5 kHz at 300 K for (a) hydrated sulfated SBA-15 with 5% $ZrO_2$, (b) dehydrated sulfated SBA-15 with 5% $ZrO_2$, (c) hydrated sulfated SBA-15 with 30% $ZrO_2$, (d) dehydrated sulfated SBA-15 with 30% $ZrO_2$.

hydrated sulfated ones at different $ZrO_2$ contents (figure 5). At $ZrO_2$ levels greater than ca. 20%, two intense peaks at ca. 1.2 and 3.8 ppm typical of OH shifts of crystalline $ZrO_2$ (figure 5c) are observed. These shifts are in good agreement with the shifts reported by Riemer *et al.* [28]. It is important to note here that at 25% $ZrO_2$ loading the crystalline zirconia peaks also appeared in the XRD patterns, indicating the formation of $ZrO_2$ crystals (figure 1). Moreover, the $^1$H MAS NMR spectra of the hydrated samples also allow a very clear conclusion about the superacid sites: For low $ZrO_2$ content (5%) only one almost symmetric line is observed at ca. 8 ppm (figure 5a). The chemical shift of this line is slightly changed from 7.8 ppm to 8.9 ppm if the $ZrO_2$ content is increased to 30% (figure 5a and c). It is obvious that this line corresponds to the line observed at 10.6 ppm for the dehydrated samples. The chemical shift is reduced to ca. 8 ppm due to the fast exchange between protons of the adsorbed water (and, apparently, also in the structural OH groups) on the one side and protons of the superacid sites on the other side. Note that for the same reason the intensity of typical silanol lines between −0.5 ppm and 2.3 ppm (figure 5b and d), seen after the dehydration treatment, is strongly reduced or even no more detectable in case of hydrated samples. Our measurements on hydrated and dehydrated sulfated SBA-15 samples with zirconia have clearly revealed the formation of accessible superacid proton sites.

## 4. Conclusion

We have reported the preparation and the acid characteristics of sulfated zirconia included SBA-15 catalysts. Our measurements on hydrated and dehydrated sulfated zirconia included SBA-15 samples have clearly revealed the formation of accessible superacid Brønsted sites. The fine distribution of zirconia in SBA-15 structure was achieved up to 25 mol% $ZrO_2$ included catalyst at which the highest acidity was observed with a BET surface area of 246 $m^2/g$.

## Acknowledgements

The authors are grateful for the doctoral scholarship and exchange grants from the Scientific and Research Council of Turkey (TUBITAK) through the BDP program. We thank to Jie Fan and Galen Stucky (UC, Santa Barbara) for TEM images. This work has been supported by METU Research Fund Projects (Grant.

No: BAP-2006-03-04-05) and by the European Commission through the FP6 project called METU-CENTER under the contract FP6-2004-ACC-SSA-2-17125.

## References

[1] G.A. Olah and A. Molnar, *Hydrocarbon Chemistry* (John Wiley, New York, 1995).
[2] V. Degirmenci, D. Uner and A. Yilmaz, Catal. Today 106 (2005) 252.
[3] G.D. Yadav and J.J. Nair, Micropor. Mesopor. Mater. 33 (1999) 1.
[4] B.H. Davis, R.A. Keogh and R. Srinivasan, Catal. Today 20 (1994) 219.
[5] X. Song and A. Sayari, Catal. Rev. Sci. Eng. 38 (1996) 329.
[6] V. Adeeva, G.D. Lei and W.M.H. Sachtler, Catal. Lett. 33 (1995) 135.
[7] H. Liu, V. Adeeva, G.D. Lei and W.M.H. Sachtler, J. Mol. Catal. A 100 (1995) 35.
[8] R.A. Comelli, C.R. Vera and J.M. Parera, J. Catal. 151 (1995) 96.
[9] J.H. Wang and C.Y. Mou, Appl. Catal. A 286 (2005) 128.
[10] C.T. Kresge, M.E. Leonowicz, W.J. Roth, J.C. Vartli and J.S. Beck, Nature 359 (1992) 710.
[11] A. Sayari, Chem. Mater. 8 (1996) 1840.
[12] J.S. Beck, J.C. Vartli, W.J. Roth, M.E. Leonowicz, C.T. Kresge, K.D. Schmitt, C.T.W. Chu, D.H. Olson, E.W. Sheppard, S.B. McCullen Cu, J.B. Higgins and J.L. Schlenker, J. Am. Chem. Soc. 114 (1992) 10834.
[13] A. Corma, Chem. Rev. 97 (1997) 2373.
[14] C.L. Chen, T. Li, S. Cheng, H.P. Lin, C.J. Bhongale and C.Y. Mou, Micropor. Mesopor. Mater. 50 (2001) 201.
[15] U. Ciesla, S. Schacht, G.D. Stucky, K.K. Unger and F. Schuth, Angew. Chem. Int. Ed. Engl. 35 (1996) 539.
[16] F. Schuth, Ber. Bunsenges Phys. Chem. 99 (1995) 130.
[17] J.A. Knowles and M.J. Hudson, J. Chem. Soc. Chem. Commun. (1995) 2083.
[18] J.A. Knowles and M.J. Hudson, J. Mater. Chem. 6 (1996) 89.
[19] W. Hua, Y. Yue and Z. Gao, J. Mol. Catal. A 170 (2001) 195.
[20] M.V. Landau, L. Vradman, X. Wang and L. Titelman, Micropor. Mesopor. Mater. 78 (2005) 117.
[21] Z.G. Wu, Y.X. Zhao and D.S. Liu, Micropor. Mesopor. Mater. 68 (2004) 127.
[22] Y. Du, Y. Sun, Y. Di, L. Zhao, S. Liu and F.S. Xiao, J. Porous. Mater. 13 (2006) 163.
[23] J. Trèbosc, J.W. Wiench, S. Huh, V.S.Y. Lin and M. Pruski, J. Am. Chem. Soc. 127 (2005) 3057.
[24] M.D. Alba, A.I. Becerro and J. Klinowski, J. Chem. Soc. Faraday Trans. 92 (1996) 854.
[25] H. Pfeifer, D. Freude and M. Hunger, Zeolites 5 (1985) 274.
[26] E. Brunner, *Habilitation Thesis* (University of Leipzig, 1995).
[27] E. Brunner, Catal. Today 38 (1997) 361.
[28] T. Riemer, D. Spielbauer, M. Hunger, G.A.H. Mekhemer and H. Knoezinger, J. Chem. Soc. Chem. Commun. (1994) 1181.
[29] D.Y. Zhao, Q.S. Huo, J.L. Feng, B.F. Chmelka and G.D. Stucky, J. Am. Chem. Soc. 120 (1998) 6024.
[30] D. Zhao, J. Feng, Q. Huo, N. Melosh, G.H. Fredrickson, B.F. Chmelka and G.D. Stucky, Science 279 (1998) 548.
[31] M. Pruski, J.C. Klezenberg, B.C. Gerstein and T.S. King, J. Am. Chem. Soc. 112 (1990) 4232.
[32] E. Brunner, J. Chem. Soc. Faraday Trans. 86 (1990) 3957.
[33] J.Z. Hu, J.H. Kwak, J.E. Herrera, Y. Wang and C.H.F. Peden, Solid State NMR 27 (2005) 200.
[34] M. Hunger, J. Ernst, S. Steuernagel and J. Weitkamp, Micropor. Mater. 6 (1996) 349.
[35] M. Hunger, U. Schenk, M. Breuninger, R. Glaeser and J. Weitkamp, Micropor. Mesopor. Mater. 27 (1999) 261.
[36] T. Emmler, S. Gieschler, H.H. Limbach and G. Buntkowsky, J. Mol. Struct. 700 (2004) 29.
[37] O.F. Erdem and D. Michel, J. Phys. Chem. B 109 (2005) 12054.